

Disentangle and Regularize: Sign Language Production with Articulator-Based Disentanglement and Channel-Aware Regularization

Sümeyye Meryem Taşyürek*
Hacettepe University

Tuğçe Kızıltepe†
Hacettepe University

Hacer Yalim Keleş‡
Hacettepe University

Abstract

In this work, we propose DARS LP, a simple gloss-free, transformer-based sign language production (SLP) framework that directly maps spoken-language text to sign pose sequences. We first train a pose autoencoder that encodes sign poses into a compact latent space using an articulator-based disentanglement strategy, where features corresponding to the face, right hand, left hand, and body are modeled separately to promote structured and interpretable representation learning. Next, a non-autoregressive transformer decoder is trained to predict these latent representations from sentence-level text embeddings. To guide this process, we apply channel-aware regularization by aligning predicted latent distributions with priors extracted from the ground-truth encodings using a KL-divergence loss. The contribution of each channel to the loss is weighted according to its associated articulator region, enabling the model to account for the relative importance of different articulators during training. Our approach does not rely on gloss supervision or pretrained models, and achieves state-of-the-art results on the PHOENIX14T and CSL-Daily datasets.

1. Introduction

Sign language serves as the primary mode of communication for Deaf and Hard-of-Hearing (DHH) individuals, relying on a rich combination of manual (hand movements) and non-manual (facial expressions, body posture) features. With the rise of deep learning, SLP has gained attention as a task that aims to generate sign language sequences from spoken language text. However, producing realistic and continuous sign language sequences remains a challenging problem due to the complex spatial-temporal nature of sign articulation.

Recent advances in SLP have focused on generating skeletal pose sequences instead of synthesizing sign language videos directly. This intermediate representation

provides a structured and computationally efficient way to model sign articulation while separating the challenges of motion synthesis and realistic rendering [19]. Despite progress, generating natural and expressive sign pose sequences remains an open challenge. Many SLP models tend to produce averaged movements, failing to capture the fine-grained articulations required for natural sign language expressions [30], [17]. This results in overly simplified gestures, particularly in hand and finger movements. Additionally, error accumulation in autoregressive decoding, where errors propagate over time, further degrades sequence coherence, leading to unnatural transitions between signs [20], [21]. To address these challenges, various techniques have been explored, including adversarial training, progressive transformers, and mixture density networks (MDNs) [22]. While these methods improve realism, they struggle with smooth and expressive sign transitions, particularly in fine hand articulations.

A significant research direction in SLP involves reducing dependency on gloss annotations, which traditionally serve as an intermediate representation between spoken and sign language. While gloss-based models achieve high accuracy, gloss annotation is costly, time-consuming, and often inconsistent across datasets, making large-scale deployment impractical. To overcome this limitation, gloss-free SLP has gained attention, aiming for direct text-to-sign generation without requiring gloss annotations [11, 30, 34]. While promising, these models still struggle with smooth transitions and expressive signing.

To address these challenges, we propose DARS LP, a simple transformer-based SLP framework that directly translates spoken language text into continuous sign pose sequences without gloss supervision. The contribution of our work to the SLP domain can be summarized as follows:

- We introduce an **articulator-based disentanglement** mechanism implemented via a pose autoencoder, where features corresponding to the face, right hand, left hand, and body are explicitly separated into distinct channel groups. This structured representation enables selective weighting of articulators (e.g., emphasizing hand movements) and facilitates the estimation of articulator-

*meryemtasyurek@cs.hacettepe.edu.tr

†tugcekiziltepe@hacettepe.edu.tr

‡hacerkeles@cs.hacettepe.edu.tr

specific latent statistics. To the best of our knowledge, this straightforward yet effective inductive bias has not been previously explored in the context of SLP.

- We propose a **channel-aware regularization** strategy for training the non-autoregressive transformer by aligning predicted latent distributions with articulator-weighted channel priors derived from the autoencoder. In contrast to common variational methods that impose prior constraints, our approach directly computes these priors from observed channel distributions. Empirical results show that this regularization improves motion diversity and realism, and effectively reduces the regression-to-the-mean problem in generated pose sequences.

Unlike previous approaches that rely on gloss supervision, our model removes the need for gloss annotations while surpassing both gloss-based and gloss-free models in back-translation performance, achieving state-of-the-art results. Our model ranked third in the CVPR 2025 SLRTP Challenge [31], demonstrating its effectiveness in producing accurate pose generation in sign language.

2. Related Work

Sign language production aims to generate sign language sequences corresponding to a given spoken language text. Recently, studies have focused on converting input text into skeletal pose sequences instead of directly synthesizing sign language videos, as this intermediate representation is more practical and generalizable [19]. The synthesis of realistic videos from these pose sequences is considered a separate research challenge. In our study, we also concentrate on generating realistic pose sequences.

One of the primary challenges in continuous SLP, akin to continuous sign language translation (SLT), stems from the lack of one-to-one alignment between spoken language and sign language sequences. Producing natural and continuous sign language sequences is significantly more complex than simply concatenating isolated signs. Ensuring a smooth transition between signs while preserving semantic integrity is crucial for achieving realistic sign flow. However, existing SLP models struggle to model these transitions effectively.

2.1. Autoregressive Approaches

A major unsolved problem in SLP research is regression to the mean, a phenomenon in which generated sign sequences converge to average motion patterns, resulting in unnatural and overly simplified gestures [30], [17]. This issue reduces the expressiveness of generated signs, particularly in hand and finger movements, leading to deviations from the intended semantic content. Consequently, sign language users may find the generated sequences difficult to understand, lowering communication quality. Addressing

this fundamental issue is essential to improve the realism and effectiveness of SLP systems.

The field of SLP has seen significant advancements since the pioneering work of Stoll et al. (2018), who used a neural machine translation (NMT) model to convert text to gloss sequences [23]. However, these early approaches were insufficient for producing natural and continuous sign language sequences. Later, Saunders et al. (2020a) introduced a transformer-based continuous SLP model. Despite improvements, the autoregressive nature of transformer-based models exacerbated the regression-to-the-mean issue, limiting their ability to capture fine details [20]. To mitigate this, Saunders et al. (2020b) incorporated adversarial training with a multichannel sign production framework. Although this approach systematically addressed the regression-to-the-mean problem for the first time, it did not fully resolve it [21].

Later methods such as progressive transformers and mixture density networks (MDN) have been explored, combined with data augmentation and adversarial training techniques [22]. Despite these efforts, user evaluations indicate that the regression-to-the-mean problem persists. While MDN models attempt to model the natural variation in sign sequences, they fail to capture fine-grained finger movements, resulting in incorrect articulation patterns.

2.2. Non-Autoregressive Approaches

To overcome these limitations autoregressive approaches, Hwang et al. (2021) introduced the NSLP-G model [9]. This model encoded signs in a Gaussian space using a VAE framework to generate poses directly. However, NSLP-G struggled to predict sequence length and failed to capture fine-grained finger details effectively. Hwang et al. (2022) later proposed length regulators and knowledge distillation techniques to address these issues [10]. By replacing MSE loss with binary cross-entropy (BCE), they improved the capture of low-variance details. However, the challenge of representing fine hand and finger articulations in the latent space remains unresolved. The VAE encoder, despite producing distinct latent vectors, lacks the capacity to fully encode the intricacies of hand poses. The decoder tends to focus on reconstructing larger body structures while neglecting hand details.

Ma et al. (2024) tackled the regression-to-the-mean issue by introducing a dual-decoder transformer, designed to improve hand modeling in SLP. Their approach employed a separate decoder for manual features (hand poses) alongside the full-body pose decoder to ensure better alignment. While this method showed improvements in hand articulation, it also revealed critical challenges. The model’s performance suffered due to the scarcity of high-quality training data, particularly for complex hand poses. Moreover, the dual-decoder structure increased computational costs and

was highly sensitive to dataset quality, limiting its generalizability [17].

2.3. Gloss-Free Approaches

While gloss-based SLP models achieve higher accuracy, gloss annotation is costly and time-consuming, limiting scalability. To address this, gloss-free approaches aim to translate spoken language directly into sign language sequences without gloss labels. Hwang et al. (2024) introduced SignVQNet [11], which employs an autoregressive structure by converting sign pose sequences into discrete tokens. Similarly, Walsh et al. (2024) leveraged vector quantization (VQ) to reduce gloss dependency. However, VQ-based discrete tokenization often results in unnatural transitions and loss of fine details in complex sign motions [29, 30]. Yin et al. (2024) proposed Dynamic Vector Quantization (DVQ-VAE), which adjusts encoding length based on information density [34]. Despite improvements, VQ-based methods still struggle with smooth sign transitions, and error accumulation in autoregressive models remains a challenge.

To alleviate the limitations posed by gloss annotations, several alternative intermediate representations have been proposed. Systems such as the Hamburg Notation System (HamNoSys) [7] and SignWriting [24] aim to capture phonetic or visual aspects of sign language and have been explored as substitutes for glosses in sign language production pipelines. For instance, HamNoSys, which encodes signs at the articulatory level, can be directly mapped to avatars and has been utilized in the Text-to-HamNoSys (T2H) task, showing improved translation performance [28]. Similarly, recent work has investigated SignWriting-based translation and synthesis pipelines [1, 14]. However, these systems still rely on specialized, manually annotated symbolic representations and suffer from similar scalability challenges as gloss-based models.

Given the data scarcity and annotation bottlenecks in sign language datasets our work follows an alternative paradigm by completely bypassing gloss-level supervision. We propose a gloss-free sign language production framework that learns to generate continuous sign pose sequences directly from spoken language inputs, enabling scalable and end-to-end learning without the need for intermediate linguistic annotations.

2.4. Latent Space Modeling and Disentanglement

Beyond discrete tokenization, some studies explored continuous latent space modeling, often using autoencoders or variational methods [9, 10]. These works attempt to learn compact, expressive embeddings that preserve both manual and non-manual features. However, they often treat pose data holistically, failing to separate the dynamics of distinct articulators. This design leads to inefficient representation

of subtle articulations, particularly for hands and fingers. Since these models operate in a Gaussian latent space, they tend to capture global patterns while underrepresenting low-variance, fine-grained features.

Beyond the SLP domain, significant advancements have been made in learning compact, structured latent spaces using autoencoders across diverse modalities. Autoencoders have proven effective in capturing essential data representations while reducing dimensionality, supporting tasks such as sequence modeling [4], biomedical data analysis [32], and latent variable modeling [15]. Particularly in multimodal tasks, disentangled representations are crucial to separately model different modalities’ distinct characteristics while maintaining coherence. Inspired by this, our approach incorporates a structurally disentangled autoencoder specifically tailored to the multimodal nature of sign language, where manual (hand movements) and non-manual (facial expressions, body posture) features must be modeled jointly but distinctly. Unlike prior SLP works that treat pose sequences holistically or rely heavily on discrete representations, we structure the latent space to explicitly capture the separate dynamics of different body parts.

Additionally, while KL divergence loss has been widely employed in variational autoencoders (VAEs) and sequence generation tasks to regularize latent spaces [2], its potential remains underutilized in sign language production. In this work, we investigate the usage of KL divergence as a regularization signal within a structurally disentangled latent space, designed to represent manual and non-manual articulators separately. This setup allows for targeted regularization that promotes smoothness and structural consistency across body regions, without relying on a variational framework.

3. Methodology

3.1. Pose Autoencoder

To effectively capture the multimodal structure inherent in sign language articulation, we employ a structurally disentangled pose autoencoder designed to encode and reconstruct sign poses in a compact latent space. Rather than aiming to achieve disentanglement in the strict unsupervised sense, we explicitly incorporated an architectural design that encourages the model to learn semantically organized representations. This design introduces a multi-modal latent factorization that aligns well with the physical structure and functional roles of each body part in sign language expression. The model operates on 3D skeleton sequences from the normalized version of the PHOENIX2014T dataset. Each input sequence consists of 50 upper body and hand joints alongside 128 facial keypoints, where each keypoint is represented by its (x, y, z) coordinates.

The encoder architecture shown in Figure 1 is explicitly

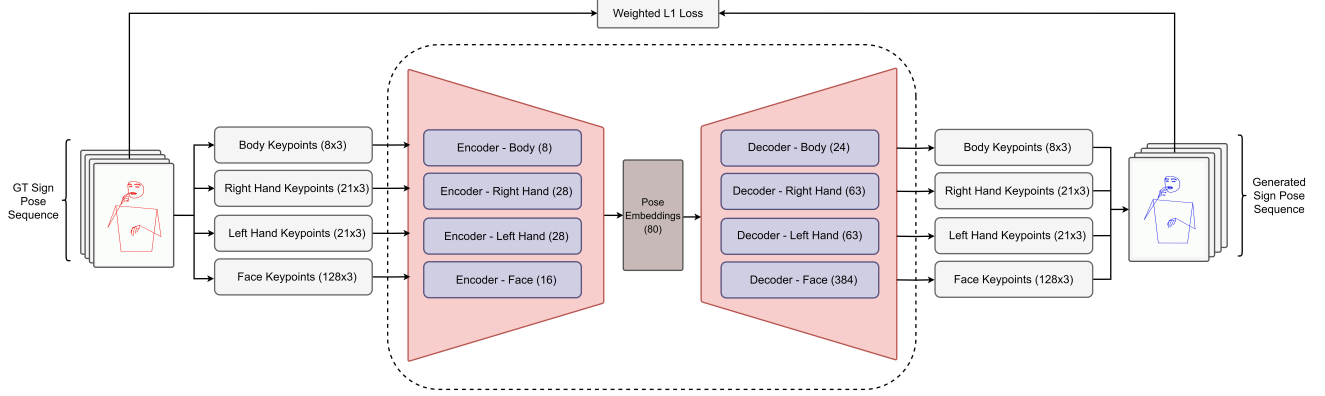


Figure 1. Overview of the proposed pose autoencoder architecture.

partitioned to process four anatomically distinct regions: upper body, right hand, left hand, and face. Each region is assigned to a dedicated linear encoder. The latent representation is an 80-dimensional vector, within which the face component is fixed at 16 dimensions, and the remaining 64 dimensions are distributed between the upper body and hands. The latent dimensionality is allocated proportionally based on the number of joints in each region, ensuring balanced representation. The upper body region, consisting of 8 joints, corresponding to shoulders, elbows, wrists and hips, is mapped from a 8×3 vector to an 8-dimensional latent representation. The right and left hands, each containing 21 joints, are projected from 21×3 vectors to 28-dimensional latent vectors. The face region, comprising 128×3 facial landmarks, is compressed to a 16-dimensional latent space. These configurations are selected based on ablation studies during autoencoder training, where various latent sizes are compared in terms of pose reconstruction quality. Although a higher-dimensional space yielded slightly better performance, we selected the 80-dimensional configuration to maintain a compact latent representation, considering the limited size of training datasets typically available in the sign language domain.

The design choice to represent the face with only 16 dimensions, despite its high raw dimensionality, is grounded in our analysis of the keypoint variance for the landmarks, a significant portion of the facial keypoints exhibit highly correlated movement patterns, particularly in areas such as the cheeks, jawline, and forehead. These regions tend to move coherently during sign articulation, resulting in lower intrinsic variability. Consequently, the face keypoints form a manifold with lower effective dimensionality. By exploiting this redundancy, the encoder achieves a high compression rate without compromising reconstruction quality.

The decoder mirrors the encoder structure, reconstructing the original pose sequences from the structured latent vectors of each body region. To ensure high-fidelity recon-

struction, we apply a weighted L1 loss, computing reconstruction losses separately for each region. To further enforce sparsity and improve the quality of the learned latent representations, we apply L1 regularization exclusively to the encoder weights which is computed as the sum of the absolute values of all encoder weight parameters. This regularization scheme ensures that the encoder learns compact and meaningful latent codes, which contributes to improved generalization and robustness in downstream sign generation.

3.2. Transformer Model

Following the latent pose representation learned by the pose autoencoder, the second stage of our framework generates sign pose embeddings conditioned on spoken language text. To accomplish this, we utilize a Transformer-based encoder-decoder architecture that directly maps sentence-level text embeddings into the structurally disentangled latent space previously established during the first stage of pose encoder training.

The input to the transformer encoder consists of BERT-based text embeddings, where each word is represented by a 768-dimensional vector. These embeddings are projected to a 512-dimensional space through a linear transformation to align with the transformer’s internal dimensionality. The encoder comprises 3 layers, each equipped with 4 attention heads and a 1024-dimensional feed-forward network, followed by positional encoding to retain temporal ordering of the text sequence.

The decoder adopts a non-autoregressive structure to alleviate error accumulation issues commonly observed in autoregressive models. It includes 6 layers with 8 attention heads, each utilizing a 1024-dimensional feed-forward network. To initialize temporal dynamics, we employ learned time queries derived from a canonical reference pose, providing a consistent starting point for generating sign sequences. The decoder outputs are processed by a linear

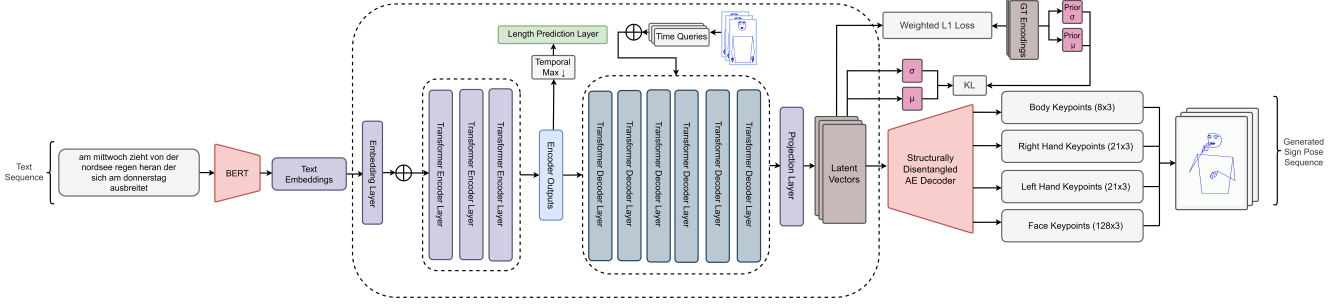


Figure 2. Overview of the proposed DAR-SLP architecture.

projection layer to reduce their dimensionality to match the 80-dimensional latent space defined by the autoencoder.

Ground truth (GT) pose encodings for transformer training are obtained by passing the training set poses through the encoder of the pretrained pose autoencoder. These encodings provide compact, structurally disentangled representations of manual (hands) and non-manual (face, upper body) articulators, guiding the transformer model to learn structured mappings from spoken language text to continuous sign pose sequences. To enforce accurate reconstruction of these latent encodings, we apply L1 loss between the transformer’s predicted embeddings and the GT encodings.

Furthermore, to ensure that generated latent representations align with the distributional characteristics of the autoencoder’s latent space, we introduce a KL divergence-based regularization later in training. Specifically, prior distributions for each articulatory region, precomputed from the autoencoder, serve as reference distributions guiding the Transformer’s predictions. This approach promotes consistency and structural coherence in the generated embeddings, enhancing generalization to unseen inputs by maintaining fidelity to the learned latent space distribution.

To align the duration of generated sign sequences with the complexity of the input sentences, we integrate a length predictor module into our framework. Specifically, the Transformer encoder outputs are pooled into a sentence-level embedding, which is then passed through a linear layer with sigmoid activation to predict a normalized length ratio between 0 and 1. This ratio corresponds to the proportion of the maximum possible sequence length required to represent the given input sentence. During inference, the predicted length ratio dynamically determines the actual sequence length by selecting the corresponding number of frames from the decoder’s output. The length predictor is trained using supervision from ground-truth sequence lengths, thereby promoting temporal coherence and improving the synchronization of generated sign motion with the input sentences. This also ensures that the rhythm and extent of sign motion appropriately reflect the sentence’s semantic load. This idea is further supported by previous

work [34], which demonstrate a strong correlation between input sentence length and video duration, highlighting the importance of conditioning generation length on input characteristics.

As shown in Figure 2, after the transformer generates the predicted pose embeddings, the sequence of 3D pose keypoints can be readily reconstructed by passing the output embeddings through the decoder of the pretrained pose autoencoder obtained in the first stage. This design enables efficient end-to-end generation of complete sign pose sequences without requiring additional refinement or post-processing steps.

4. Experiments

4.1. Datasets

We evaluate our model on two continuous sign language datasets. PHOENIX-2014T [3] contains 8,247 German Sign Language sentences aligned with gloss and spoken German. We use the 3D pose annotations from the CVPR 2025 SLRTP Challenge [31], where 2D keypoints extracted via MediaPipe Holistic [16] are uplifted to 3D using Ivashechkin *et al.*’s method [13], yielding $N \times 178 \times 3$ tensors. CSL-Daily [35] includes 20,654 Chinese Sign Language (CSL) sentences from 10 signers. We extract 3D poses using MediaPipe Holistic, standardizing each frame to 178 keypoints (upper body, hands, face). To ensure consistency across signers and datasets, poses are normalized by centering on the neck and scaling by shoulder width.

4.2. Training Procedure

Our training strategy follows a two-stage process to effectively map spoken language sentences to continuous sign pose sequences. In the first stage, we train a structurally disentangled pose autoencoder to learn compact multi-modal latent representations of sign language poses. The autoencoder is optimized to accurately reconstruct the original poses while ensuring meaningful decomposition of manual (hands) and non-manual (face, upper body) articulators. In the second stage, we train a non-autoregressive transformer

to predict these latent pose representations conditioned on the input text. This stage utilizes sentence embeddings and is supervised with the ground truth encodings produced by the pretrained pose encoder.

4.2.1. Training the Pose Autoencoder

The training objective of our structurally disentangled autoencoder is to minimize the weighted reconstruction loss across four distinct anatomical regions: upper body, right hand, left hand, and face. The reconstruction loss for each region is computed independently using the L1 loss function, reflecting the absolute difference between the input keypoints and their reconstructions. The total loss is computed as the weighted sum of these individual components. The weights are set to 1.5 for both hands, reflecting their critical role in manual articulation, and 0.5 and 1.0 for the upper body and face, respectively. The reason we down-scale the weight of upper body joints is to prevent the loss function from being dominated by high-variance, large-scale motions, which can lead the model to overlook fine-grained but semantically important hand and facial movements. The total loss is provided in (1).

$$\mathcal{L}_{recon} = \sum_{r \in \{B, RH, LH, F\}} w_r \frac{1}{N_r} \sum_{i=1}^{N_r} \|\hat{\mathbf{x}}_r^{(i)} - \mathbf{x}_r^{(i)}\|_1 \quad (1)$$

where; $\mathbf{x}_r^{(i)}$ and $\hat{\mathbf{x}}_r^{(i)}$ denote the ground truth and reconstructed keypoints for region r at frame i , N_r is the total number of frames, w_r is the weight assigned to region r , set empirically as $w_B = 0.5$, $w_{RH} = 1.5$, $w_{LH} = 1.5$, and $w_F = 1.0$. The regions B, RH, LH, F represent body, right hand, left hand and face channels, respectively.

$$\mathcal{L}_{reg-enc} = \lambda \sum_{j \in \{enc\}} \|\mathbf{W}_j\|_1 \quad (2)$$

To encourage sparsity in the latent representations and prevent overfitting, we apply an L1 regularization term to the encoder weights. The regularization coefficient (λ) is set empirically to 1×10^{-4} based on cross-validation. Applying L1 regularization solely to the encoder, while leaving the decoder unregularized, is a strategy adopted in sparse autoencoders [18], [27]. By not constraining the decoder, we retain its full capacity to reconstruct the fine-grained spatial dependencies inherent in sign articulation, particularly in manual articulators such as fingers. In contrast, imposing sparsity on the decoder could unnecessarily limit its expressiveness and compromise reconstruction fidelity.

The total autoencoder loss function combines reconstruction and regularization terms:

$$\mathcal{L}_{total-ae} = \mathcal{L}_{recon} + \mathcal{L}_{reg-enc} \quad (3)$$

Optimization is performed using the Adam optimizer, with a learning rate of 2×10^{-4} and beta parameters set to (0.5, 0.9), ensuring stable convergence during training.

4.2.2. Training Generator Model

The training objective of our transformer model is divided into two phase to effectively balance the learning of accurate pose encodings and structured latent space distribution. In the first-phase, the model is trained to predict ground truth (GT) pose encodings obtained from the pretrained pose autoencoder. In this phase, we minimize an L1 loss between the predicted encodings for the transformer model and the obtained GT encodings. We will refer to this model as DARSPLP.

For a sequence of length T , the total pose encodings loss is defined as:

$$\mathcal{L}_{enc} = \sum_{R \in \{B, RH, LH, F\}} w_R \frac{1}{T} \sum_{t=1}^T \|\hat{z}_t^{(R)} - z_t^{(R)}\|_1 \quad (4)$$

where $\hat{z}_t^{(R)}$ and $z_t^{(R)}$ are the predicted and GT encodings at timestep t , and w_R denotes region-specific weights. We empirically set $w_B = 1$, $w_{RH} = 7$, $w_{LH} = 5$, $w_F = 2$, emphasizing the importance of manual articulators.

Since hands carry the core lexical content in sign language, they are given the highest weights ($w_{RH} = 7$, $w_{LH} = 5$). The right hand, in particular, is typically the dominant hand in sign languages like DGS and CSL, and is primarily responsible for conveying meaning, while the left hand often plays a supportive or symmetrical role. The body provides broader spatial cues but is less semantically dense per frame, so it has a lower weight ($w_B = 1$). The face, while critical for grammatical and emotional expressions, involves highly redundant motion across many keypoints, leading to a moderate weight ($w_F = 2$). This design ensures the model focuses on the most informative regions for sign language generation.

In addition, the model predicts the relative sequence length, supervised by an L1 length loss:

$$\mathcal{L}_{len} = \|\hat{r} - r\|_1 \quad (5)$$

where, \hat{r} is the predicted length ratio, and r is the ground truth. The overall objective in this phase becomes:

$$\mathcal{L}_{phase1} = \mathcal{L}_{enc} + \mathcal{L}_{len} \quad (6)$$

In the second phase of transformer training, we incorporate a KL divergence term to promote generalization and preserve the distributions of the structurally disentangled latent space. We refer to the resulting model as DARSPLP-KL,

which extends the first-phase model by adding regularization on the prior channel distributions. In this context, during training, we enforce the predicted latent channel distributions to align with precomputed priors derived from ground truth encodings for each articulator region. This loss term is provided in Eqn. (7).

$$\mathcal{L}_{\text{KL}} = \sum_R \lambda_R \sum_{c \in R} D_{\text{KL}} \left(\mathcal{N}(\mu^{(c)}, \sigma^{(c)}) \parallel \mathcal{N}(\mu_{\text{prior}}^{(c)}, \sigma_{\text{prior}}^{(c)}) \right) \quad (7)$$

Here, $\mu^{(c)}$ and $\sigma^{(c)}$ denote the batch-wise mean and variance of the predicted encoding channels, computed dynamically at each training iteration, while $\mu_{\text{prior}}^{(c)}$ and $\sigma_{\text{prior}}^{(c)}$ represent the prior statistics derived from the training data embeddings. Here, R is the similar region set $\{B, RH, LH, F\}$ that we explained previously, and each channel is weighted according to the region it belongs to. For initial experiments we set the weights as $\lambda_B = 1$, $\lambda_{RH} = 5$, $\lambda_{LH} = 3$, $\lambda_F = 1$.

The total loss in this phase becomes as in Eqn. (8).

$$\mathcal{L}_{\text{phase2}} = \mathcal{L}_{\text{enc}} + \mathcal{L}_{\text{len}} + \mathcal{L}_{\text{KL}} \quad (8)$$

We employ the Adam optimizer with a learning rate of 2×10^{-4} , weight decay of 1×10^{-4} , and a ReduceLROnPlateau scheduler (factor 0.9, patience 40). Early stopping based on validation loss is applied to prevent overfitting. Our model is implemented using PyTorch Lightning [5], trained on a HPC with 4 NVIDIA A100-SXM4-40GB GPU.

4.3. Ablations

Ablation study on latent dimensionality. To assess the impact of latent dimensionality on sign pose generation, we conduct an ablation study by varying the allocation of dimensions across body, hands, and face components. These experiments test whether increased capacity improves downstream performance and validate our design choices. We compare three configurations: (1) 80 dimensions (64 for body and hands, 16 for face), (2) 96 dimensions (64 + 32), and (3) 160 dimensions (128 + 32). Within each, body and hand dimensions are distributed proportionally to joint counts to maintain anatomical consistency.

As shown in Table 1, the 80-dimensional setup achieves the best overall performance. Increasing face capacity to 32 dimensions shows no gain, while expanding body and hand dimensions to 128 degrades results. The ablation further validates our face encoding decision. We demonstrated that the 128×3 facial keypoints, due to their strong inter-keypoint dependency, can be effectively compressed to just 16 latent dimensions without compromising accuracy. This structural redundancy in facial movements, confirmed by our variance analysis enables robust and efficient encoding

(see Section 5.1). Increasing the dimensionality beyond this point introduces unnecessary capacity without a gain, confirming the compact configuration as both sufficient and optimal.

Ablation study on generator training. To determine the optimal setup for our transformer-based generator, we conducted ablation studies on training strategies and region-wise weighting. We initially used moderate region weights (1–7–5–2) for the L1 loss and (1–3–5–1) for the KL divergence, corresponding to the body, right hand, left hand, and face regions, respectively, to reflect articulator importance without imposing a strong bias. This served as a baseline for assessing the impact of KL regularization and its scheduling. As shown in Table 2, omitting KL leads to suboptimal performance (BLEU-4: 7.59), while applying it from the start causes instability (BLEU-4: 6.93). Our two-stage training strategy, introducing KL after initial training, yields the best results (BLEU-4: 8.70). This aligns with findings in VAE-based models, where premature KL application can collapse the latent space toward the prior [2], prompting staged or cyclical KL schedules [6, 25]. Though our model does not learn a variational posterior, our findings suggest that latent space regularization benefits from careful scheduling of KL divergence even in deterministic, structured representation settings.

After establishing the training pipeline with this balanced setup, we performed further ablations focusing on region-specific weighting. These experiments explore how emphasizing specific articulators (particularly the hands) in both L1 and KL terms influences the generation quality (Tables 3 and 4).

Based on the ablation results, **region-wise L1 loss weights are set to (1–14–10–2)**, and KL divergence is introduced in the **second phase with weights (1–10–6–1)**.

5. Discussions

5.1. Analysis of the Learned Latent Spaces

The statistical analysis of the learned latent representations reveals meaningful distinctions in the encoding behavior across body regions. In Figure 3, we present example histograms and corresponding entropy values for selected channel distributions from each structurally disentangled latent subspace (face, body, right hand, and left hand) learned by the autoencoder.

As can be seen, the face channels have minimal variance. In contrast, the right and left hand channels show broader, more dispersed distributions with higher entropy and standard deviation across most dimensions, confirming the rich variability and critical role of manual articulators in sign expression. The body encodings fall somewhere in between, reflecting more stable but still semantically relevant movement, however body region spans a larger phys-

Table 1. Performance comparison of the models with different latent dimensions on the PHOENIX14T DEV Set. All models are trained without KL divergence.

Models	DTW-MJE↓	BLEU-1↑	BLEU-2↑	BLEU-3↑	BLEU-4↑	chrF↑	ROUGE↑
GT	0.000	30.92	21.34	16.01	12.74	34.71	30.19
128 (Body+Hands) + 32 (Face)	0.042	22.45	13.78	9.58	7.21	28.18	20.70
64 (Body+Hands) + 32 (Face)	0.044	20.92	12.57	8.79	6.72	27.78	19.91
64 (Body+Hands) + 16 (Face)	0.041	22.59	13.87	9.83	7.59	28.25	21.19

Table 2. Performance comparison of the models with different training strategies on the PHOENIX14T DEV Set. All models use 80-dimensional latent space.

Models	DTW-MJE↓	BLEU-1↑	BLEU-2↑	BLEU-3↑	BLEU-4↑	chrF↑	ROUGE↑
GT	0.000	30.92	21.34	16.01	12.74	34.71	30.19
L1 w/o KL	0.041	22.59	13.87	9.83	7.59	28.25	21.19
L1 + w/ KL	0.042	20.51	12.46	8.88	6.93	27.00	18.95
Pretrained(w/L1)+Tuning w/ KL	0.039	25.91	16.34	11.43	8.70	29.92	23.67

Table 3. Performance comparison of models with different region weight configurations on the PHOENIX14T DEV set. All models use 80-dimensional latent space, and are trained without KL regularization.

Weighting Strategy (Body–RH–LH–Face)	DTW-MJE↓	BLEU-1↑	BLEU-2↑	BLEU-3↑	BLEU-4↑	chrF↑	ROUGE↑
Uniform (1–1–1–1)	0.039	22.14	13.14	8.95	6.72	27.89	19.91
Moderate Hand Emphasis (1–7–5–2)	0.041	22.59	13.87	9.83	7.59	28.25	21.19
Heavy Hand Emphasis (1–14–10–2)	0.043	24.78	15.84	11.26	8.66	29.36	22.98

Table 4. Ablation results with different KL divergence weights with fixed L1 weighting (1–14–10–2) on the PHOENIX14T DEV set. All models use 80-dimensional latent space, and are trained with staged KL regularization.

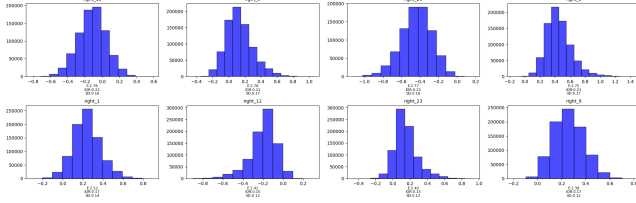
KL Weights (Body–RH–LH–Face)	DTW-MJE↓	BLEU-1↑	BLEU-2↑	BLEU-3↑	BLEU-4↑	chrF↑	ROUGE↑
Uniform (1–1–1–1)	0.040	26.69	17.49	12.79	9.99	30.63	24.92
Moderate Hand Emphasis (1–3–5–1)	0.040	27.35	17.51	12.52	9.66	30.96	25.28
Heavy Hand Emphasis (1–10–6–1)	0.039	27.11	18.00	13.09	10.27	31.38	25.70

ical space and thus generates higher magnitude latent activations, even when the underlying motion is less semantically dense. To mitigate this effect and maintain balanced learning, we increase the contribution of semantically richer regions by weighting.

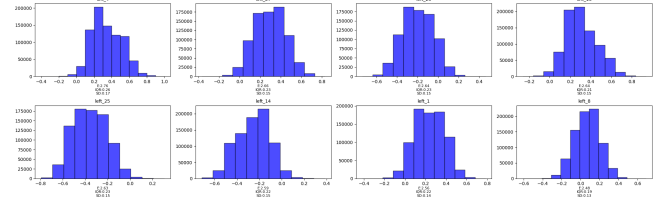
These distributional differences confirm that the latent space is semantically partitioned. They also highlight the need for targeted regularization and proper loss weighting. This encourages the model to focus more on dense, information-rich regions while still preserving reconstruction quality across all articulators.

The latent space structure observed in CSL-Daily mirrors that of PHOENIX14T, with clear separation between articulator groups and similar relative entropy patterns,

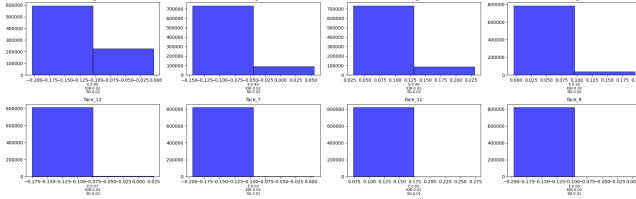
manual articulators exhibit the highest variability, followed by face and body (Figure 4). CSL-Daily encodings exhibit broader distributions across all articulator groups, as reflected by higher entropy values, particularly in the manual articulators. The left and right hand channels display the widest spread, with average entropies around 3.0, indicating increased variability and expressiveness in CSL’s daily conversational context. Even face channels, which previously showed limited variance, now present more active and information-rich distributions. This broader activation aligns with CSL-Daily’s more diverse signer pool and open-domain language, reinforcing the need for careful latent space design.



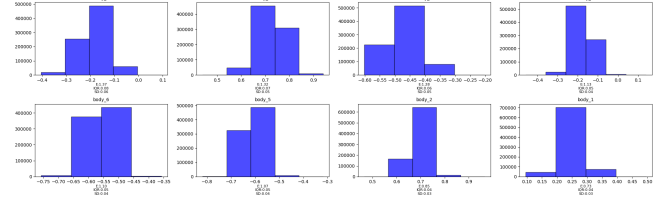
(a) Top 8 right hand channels with highest entropy. Average entropy across all channels: 2.0101.



(b) Top 8 left hand channels with highest entropy. Average entropy across all channels: 2.2241.

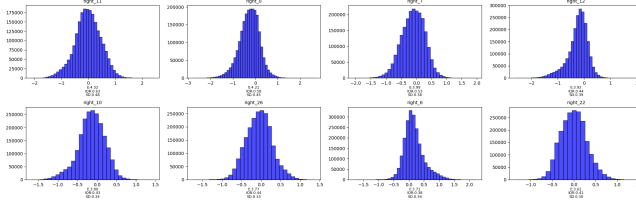


(c) Top 8 face channels with highest entropy. Average entropy across all channels: 0.1377.

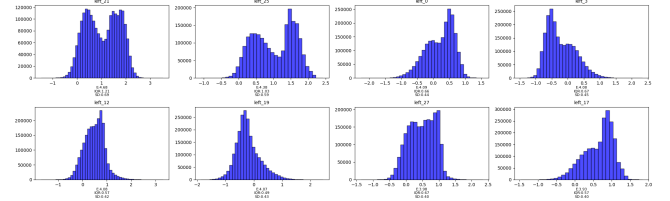


(d) Top 8 body channels with highest entropy. Average entropy across all channels: 1.1075.

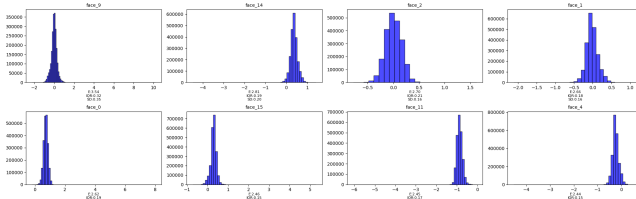
Figure 3. Histograms of top 8 latent channels with the highest entropy for each region. Each subplot shows the distribution of a channel along with its entropy (E), interquartile range (IQR), and standard deviation (SD). (Zoom in for better visibility.)



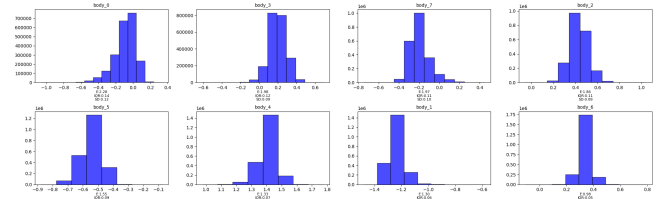
(a) Right hand channels (avg. entropy: 2.98).



(b) Left hand channels (avg. entropy: 3.19).



(c) Face channels (avg. entropy: 2.21).



(d) Body channels (avg. entropy: 1.65).

Figure 4. Histograms of top 8 latent channels with the highest entropy for each region of CSL-Daily Dataset. Each subplot shows the distribution of a channel along with its entropy (E), interquartile range (IQR), and standard deviation (SD). (Zoom in for better visibility.)

5.2. Test Results

We evaluate the best model configuration on the PHOENIX14T and CSL-Daily test sets. Table 5 presents PHOENIX14T results alongside prior work. The DARSPLP model, already outperforms several baselines, demonstrating the effectiveness of using ground-truth encodings from the autoencoder. Adding KL divergence in the second phase significantly improves generalization by reducing overfit-

ting to dominant high-variance patterns (e.g., body motion) and encouraging smoother outputs aligned with latent region distributions. This yields measurable gains: BLEU-4 improves from 8.86 to 10.90 and ROUGE from 28.50 to 31.80, confirming the benefit of aligning predicted embeddings with learned priors.

Sample pose sequences are illustrated in Figure 5. As observed in these qualitative examples, the predicted se-

Table 5. Performance comparison of the models on the PHOENIX14T TEST Set. \dagger denotes that the scores are obtained using the back translation model shared in [SLRTP-Sign-Production-Evaluation](#) [31].

Models	Gloss	DTW-MJE↓	BLEU-1↑	BLEU-2↑	BLEU-3↑	BLEU-4↑	ROUGE↑	chrF↑
GT	-	0.000	34.43	22.08	16.13	12.81	35.22	34.62
<i>Autoregressive Approaches</i>								
PT Base [30]	✓	0.197	6.27	3.33	2.14	1.59	14.52	9.50
PT FP&GN [30]	✓	0.191	11.45	7.08	5.08	4.04	19.09	14.52
G2P-MP [33]	✓	0.146	15.43	10.69	8.26	6.98	-	-
G2P-DDM [33]	✓	0.116	16.11	11.37	9.22	7.50	-	-
SignVQNet [12]	✗	0.299	-	-	-	6.88	-	-
Stitching T2P (Continuous) [30]	✗	0.572	25.14	13.54	8.98	6.67	29.5	26.49
GCDM [26]	✓	-	22.03	14.21	10.16	7.91	23.20	-
<i>Non-Autoregressive Approaches</i>								
NSLP-G [12]	✗	0.638	-	-	-	5.56	-	-
NSLP-G w/o Finetuning [12]	✗	0.646	-	-	-	4.41	-	-
NAT-AT [8]	✓	0.177	14.26	9.93	7.11	5.53	18.72	-
NAT-EA [8]	✓	0.146	15.12	10.45	7.99	6.66	19.43	-
NSVQ+Non-Autoreg. Decoding [29]	✗	0.105	27.74	16.36	11.75	9.20	27.93	-
<i>Ours-DARSLP</i> \dagger	✗	0.043	28.91	16.45	11.52	8.86	28.50	28.84
<i>Ours-DARSLP-KL</i> \dagger	✗	0.039	32.33	19.84	14.07	10.90	31.80	32.00

quences approximate the overall structure of the ground truth, reflecting key manual and non-manual articulations. While the outputs are not frame-perfect reproductions, they generally preserve the semantic intent and flow of the original signing. Despite relying on a non-autoregressive decoder, the model is able to produce smooth transitions and plausible motion patterns, suggesting that the proposed representation and training approach effectively support expressive sign generation. Importantly, these results are achieved without any gloss supervision or pretrained models, using only the PHOENIX14T training set. This demonstrates the potential of our lightweight, data-efficient framework in producing competitive results under limited supervision.

Generalization to CSL-Daily. We evaluate our finalized transformer model, selected on PHOENIX14T, on the CSL-Daily dataset using the same architecture and training strategy. To accommodate CSL-Daily’s broader linguistic context and higher variance, we added another projection layer when mapping keypoints to the 80-dimensional latent space. This produced latent distributions, particularly for the right hand, that aligned more closely with the assumed Gaussian prior, making KL regularization more effective (see Supplementary Material for details). As shown in Table 6, the model with KL divergence regularization outperforms the variant trained without KL across all met-

rics. Despite the domain shift, our model achieves competitive BLEU and ROUGE scores relative to ground-truth, which sets an upper-bound, demonstrating strong generalization to new language content and signer variability. As no prior SLP results exist for sign pose generation task on this dataset, we compare our performance against the ground truth (GT) baseline.

6. Conclusions

In this work, we presented a gloss-free sign language production framework that integrates context-aware text encoding, a semantically structured latent pose space, and dynamic temporal control within a unified architecture. At the core of our approach is a disentangled representation that separates pose features into meaningful regions, such as hands, face, and body, allowing the model to capture manual and non-manual dynamics more effectively. This design enhances representation quality and supports more interpretable modeling of sign language motion.

Our non-autoregressive transformer architecture leverages sentence-level BERT embeddings alongside a dedicated length prediction module, which dynamically adjusts the output sequence length based on the linguistic complexity of the input. This design facilitates temporal alignment between the source text and the generated sign pose sequences.

Table 6. Evaluation results on the CSL-Daily TEST Set using the finalized configuration.

Model	DTW-MJE↓	BLEU-1↑	BLEU-2↑	BLEU-3↑	BLEU-4↑	ROUGE↑	chrF↑
GT	0.000	21.63	10.90	6.31	4.02	21.81	5.26
<i>DARSLP</i>	0.177	19.13	8.33	4.46	2.73	18.72	4.24
<i>DARSLP-KL</i>	0.176	20.03	9.16	5.25	3.35	19.41	4.61

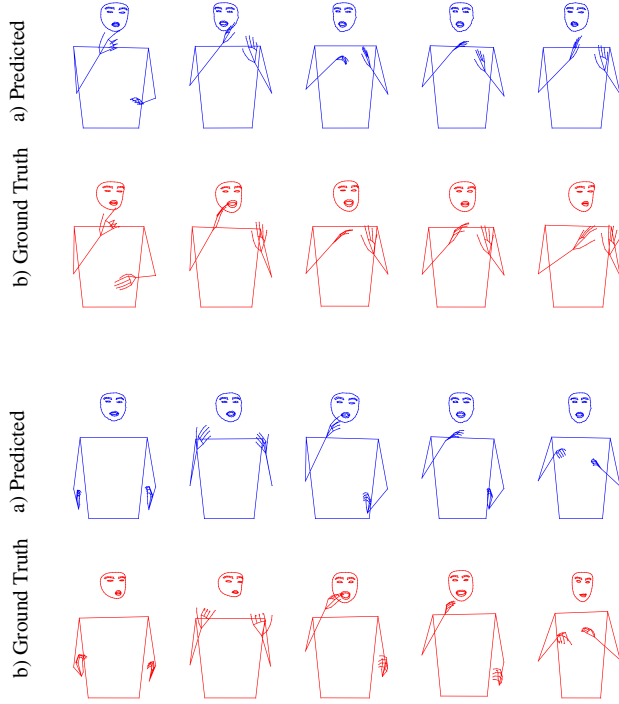


Figure 5. Pose sequences generated from input sentences. Top: "am mittwoch zieht von der nordsee regen heran der sich am donnerstag ausbreitet". Bottom: "und nun die wettervorhersage für morgen donnerstag den siebzehnten dezember".

Furthermore, we investigate the use of KL divergence to align predicted latent distributions with ground truth embedding statistics, serving as an effective regularizer within the structurally factorized latent pose space. Through two-stage training, we empirically show that introducing KL divergence after initial training helps preserve expressiveness in the learned latent representations and plays a key role in reducing the regression-to-the-mean problem, leading to more diverse and expressive sign motion generation.

Despite the absence of gloss supervision and the use of pretrained foundation models, our framework offers a lightweight yet effective solution. Compared to more complex approaches in the literature, it achieves competitive

performance through a compact architecture and a targeted training strategy.

Acknowledgements

This research is funded by TÜBİTAK under the 1001 program (grant no: 124E618). We also acknowledge the EuroHPC Joint Undertaking for awarding us access to the Vega supercomputer at IZUM, Slovenia.

References

- [1] Yosra Bouzid and Mohamed Jemni. An avatar based approach for automatically interpreting a sign language notation. pages 92–94, 2013. 3
- [2] Samuel R. Bowman, Luke Vilnis, Oriol Vinyals, Andrew M. Dai, Rafal Józefowicz, and Samy Bengio. Generating sentences from a continuous space. *CoRR*, abs/1511.06349, 2015. 3, 7
- [3] Necati Cihan Camgoz, Simon Hadfield, Oscar Koller, Hermann Ney, and Richard Bowden. Neural sign language translation. In *2018 IEEE/CVF Conference on Computer Vision and Pattern Recognition*, pages 7784–7793, 2018. 5
- [4] Andrew M. Dai and Quoc V. Le. Semi-supervised sequence learning, 2015. 3
- [5] William Falcon and The PyTorch Lightning team. PyTorch Lightning, 2019. 7
- [6] Hao Fu, Chunyuan Li, Xiaodong Liu, Jianfeng Gao, Asli Celikyilmaz, and Lawrence Carin. Cyclical annealing schedule: A simple approach to mitigating KL vanishing. In *Proceedings of the 2019 Conference of the North American Chapter of the Association for Computational Linguistics: Human Language Technologies, Volume 1 (Long and Short Papers)*, pages 240–250, Minneapolis, Minnesota, 2019. Association for Computational Linguistics. 7
- [7] Thomas Hanke. Hamnosys – representing sign language data in language resources and language processing contexts. 2004. 3
- [8] Wencan Huang, Wenwen Pan, Zhou Zhao, and Qi Tian. Towards fast and high-quality sign language production. In *Proceedings of the 29th ACM International Conference on Multimedia*, page 3172–3181, New York, NY, USA, 2021. Association for Computing Machinery. 10
- [9] Eui Jun Hwang, Jung-Ho Kim, and Jong C. Park. Non-autoregressive sign language production with gaussian space. In *The 32nd British Machine Vision Conference*

- (BMVC 21). British Machine Vision Conference (BMVC), 2021. [2](#), [3](#)
- [10] Eui Jun Hwang, Jung Ho Kim, Suk Min Cho, and Jong C. Park. Non-autoregressive sign language production via knowledge distillation, 2022. [2](#), [3](#)
- [11] Eui Jun Hwang, Huije Lee, and Jong C. Park. A gloss-free sign language production with discrete representation. In *2024 IEEE 18th International Conference on Automatic Face and Gesture Recognition (FG)*, pages 1–6, 2024. [1](#), [3](#)
- [12] Eui Jun Hwang, Huije Lee, and Jong C. Park. Autoregressive sign language production: A gloss-free approach with discrete representations, 2024. [10](#)
- [13] Maksym Ivashechkin, Oscar Mendez, and Richard Bowden. Improving 3d pose estimation for sign language, 2023. [5](#)
- [14] Zifan Jiang, Amit Moryossef, Mathias Müller, and Sarah Ebling. Machine translation between spoken languages and signed languages represented in signwriting, 2023. [3](#)
- [15] Diederik P Kingma and Max Welling. Auto-encoding variational bayes, 2022. [3](#)
- [16] Camillo Lugaresi, Jiuqiang Tang, Hadon Nash, Chris McClanahan, Esha Uboweja, Michael Hays, Fan Zhang, Chuoling Chang, Ming Guang Yong, Juhyun Lee, Wan-Teh Chang, Wei Hua, Manfred Georg, and Matthias Grundmann. Mediapipe: A framework for building perception pipelines, 2019. [5](#)
- [17] Xiaohan Ma, Rize Jin, and Tae-Sun Chung. Multi-channel spatio-temporal transformer for sign language production. In *Proceedings of the 2024 Joint International Conference on Computational Linguistics, Language Resources and Evaluation (LREC-COLING 2024)*, pages 11699–11712, Torino, Italy, 2024. ELRA and ICCL. [1](#), [2](#), [3](#)
- [18] Andrew Ng. Sparse autoencoder, 2011. CS294A Lecture notes, Stanford University. [6](#)
- [19] Razieh Rastgoo, Kourosh Kiani, Sergio Escalera, Vassilis Athitsos, and Mohammad Sabokrou. A survey on recent advances in sign language production. *Expert Systems with Applications*, 243:122846, 2024. [1](#), [2](#)
- [20] Ben Saunders, Necati Cihan Camgöz, and Richard Bowden. Progressive transformers for end-to-end sign language production. *CoRR*, abs/2004.14874, 2020a. [1](#), [2](#)
- [21] Ben Saunders, Necati Cihan Camgöz, and Richard Bowden. Adversarial training for multi-channel sign language production. *CoRR*, abs/2008.12405, 2020b. [1](#), [2](#)
- [22] Ben Saunders, Necati Cihan Camgöz, and Richard Bowden. Continuous 3d multi-channel sign language production via progressive transformers and mixture density networks. *CoRR*, abs/2103.06982, 2021. [1](#), [2](#)
- [23] Stephanie Stoll, Necati Cihan Camgöz, Simon Hadfield, and Richard Bowden. Sign language production using neural machine translation and generative adversarial networks, 2018. [2](#)
- [24] Valerie Sutton. Lessons in signwriting. 2022. [3](#)
- [25] Casper Kaae Sønderby, Tapani Raiko, Lars Maaløe, Søren Kaae Sønderby, and Ole Winther. Ladder variational autoencoders, 2016. [7](#)
- [26] Shengeng Tang, Feng Xue, Jingjing Wu, Shuo Wang, and Richang Hong. Gloss-driven conditional diffusion models for sign language production. *ACM Trans. Multimedia Comput. Commun. Appl.*, 21(4), 2025. [10](#)
- [27] Pascal Vincent, Hugo Larochelle, Isabelle Lajoie, Yoshua Bengio, and Pierre-Antoine Manzagol. Stacked denoising autoencoders: Learning useful representations in a deep network with a local denoising criterion. *J. Mach. Learn. Res.*, 11:3371–3408, 2010. [6](#)
- [28] Harry Walsh, Ben Saunders, and Richard Bowden. Changing the representation: Examining language representation for neural sign language production, 2022. [3](#)
- [29] Harry Walsh, Abolfazl Ravanshad, Mariam Rahmani, and Richard Bowden. A data-driven representation for sign language production, 2024. [3](#), [10](#)
- [30] Harry Walsh, Ben Saunders, and Richard Bowden. Sign stitching: A novel approach to sign language production, 2024. [1](#), [2](#), [3](#), [10](#)
- [31] Harry Walsh, Ed Fish, Ozge Mercanoglu Sincan, Mohamed Ilyes Lakhal, Richard Bowden, Neil Fox, Kearsy Cormier, Bencie Woll, Kepeng Wu, Zecheng Li, Weichao Zhao, Haodong Wang, Wengang Zhou, Houqiang Li, Shengeng Tang, Jiayi He, Xu Wang, Ruobei Zhang, Yaxiong Wang, Lechao Cheng, Meryem Tasyurek, Tugce Kiziltepe, and Hacer Yalim Keles. Slrtp2025 sign language production challenge: Methodology, results, and future work. In *Proceedings of the IEEE/CVF conference on computer vision and pattern recognition*, 2025. [2](#), [5](#), [10](#)
- [32] Gregory P. Way and Casey S. Greene. Extracting a biologically relevant latent space from cancer transcriptomes with variational autoencoders. *bioRxiv*, 2017. [3](#)
- [33] Pan Xie, Qipeng Zhang, Taiyi Peng, Hao Tang, Yao Du, and Zexian Li. G2p-ddm: Generating sign pose sequence from gloss sequence with discrete diffusion model, 2023. [10](#)
- [34] Aoxiong Yin, Haoyuan Li, Kai Shen, Siliang Tang, and Yuetting Zhuang. T2S-GPT: Dynamic vector quantization for autoregressive sign language production from text. In *Proceedings of the 62nd Annual Meeting of the Association for Computational Linguistics (Volume 1: Long Papers)*, pages 3345–3356, Bangkok, Thailand, 2024. Association for Computational Linguistics. [1](#), [3](#), [5](#)
- [35] Hao Zhou, Wengang Zhou, Weizhen Qi, Junfu Pu, and Houqiang Li. Improving sign language translation with monolingual data by sign back-translation, 2021. [5](#)